Advanced Materials

Pistachio-Shuck-Like MoSe2/C Core/Shell Nanostructures for High-Performance Potassium Ion Storage

--Manuscript Draft--

Manuscript Number:	adma.201801812R1
Full Title:	Pistachio-Shuck-Like MoSe2/C Core/Shell Nanostructures for High-Performance Potassium Ion Storage
Article Type:	Communication
Section/Category:	
Keywords:	Molybdenum selenide; potassium-ion battery; expanded interlayer spacing; high packing density
Corresponding Author:	Shaojun Guo Peking University Beijing, CHINA
Additional Information:	
Question	**Response**
Please submit a plain text version of your cover letter here. **If you are submitting a revision of your manuscript, please do not overwrite your original cover letter. There is an opportunity for you to provide your responses to the reviewers later; please do not add them here**.	Shaojun Guo Department of Materials Science and Engineering College of Engineering Peking University Beijing 100871, China E-mail: guosj@pku.edu.cn Mar. 10, 2018 Editors Advanced Materials Dear Editors, Enclosed please find an electronic copy of the manuscript entitled “Pistachio-Shuck-Like MoSe2/C Core/Shell Nanostructures for High-Performance Potassium Ion Storage” for your consideration as a communication to Advanced Materials. Potassium-ion batteries (KIBs) are recently attracting intensive attention in renewable energy storage system because of the abundant potassium resources and their low cost and high safety. However, the major challenge faced by KIBs lies on the lack of stable and high-capacity materials for the intercalation/deintercalation of large-size potassium ions. Transition metal selenides, with the merits of transition metal chalcogenide for batteries including high capacity, intrinsically enhanced safety and high availability through the conversion reaction, and also narrow-band-gap semiconductor characteristic, are superior anode for alkali-ion intercalation/deintercalation. However, their large volume expansion after the intercalation of large-size K ion unavoidably impacts the cycling stability of KIBs. The hollow nanostructure is an effective way in sustaining the large mechanical strain, but their packing density is relatively low due to the surplus inner void space, leading to low volumetric energy and power densities of batteries. Herein, we report the synthesis of a unique pistachio-shuck-like MoSe2/C core/shell nanostructure (PMC) as an advanced KIBs anode for boosting the performance of KIBs in terms of capacity, rate ability and cycling stability. This PMC features with a few layers of molybdenum selenide as the core with an expanded interlayer spacing of ca. 0.85 nm, facilitating the intercalation/deintercalation of K ions, and a thin amorphous carbon as the shell, which can confine the active molybdenum selenide nanosheets during cycling for maintaining the high structural stability. Most importantly, as a whole, the PMC has the advantages of reducing the surplus hollow interior space for improving its packing density and buffering the volume expansion during the K ion intercalation for further enhancing the stability. As a consequence, the PMC shows a

	very high capacity of 322 mAh g-1 at 0.2 A g-1 over 100 cycles, and can still remain 226 mAh g-1 at 1.0 A g-1 for a long period of 1000 cycles, which is among the best reported KIBs anodes. The first-principles calculations reveal that a faster diffusion of potassium ions on the layer than in the bulk molybdenum selenide and an electrical conductivity transformation from semiconductor to metal conductor after potassium intercalation are the key reasons in boosting the performance of KIBs herein. This work highlights the importance of introducing transition metal selenides as a novel anode material for KIBs and provides a new way in designing specially structured transition metal selenides/amorphous carbon composite for high-performance KIBs. We think that our paper can appeal to a broad readership that are interested in the general areas of transition-metal chalcogenides materials, nanomaterials, nanoelectrochemistry and potassium-ion batteries, and therefore will make a very important contribution to Advanced Materials. Thank you very much for your time and consideration of this manuscript. Please do not hesitate to contact me if you have any questions regarding our manuscript. Sincerely yours, Shaojun Guo
Do you or any of your co-authors have a conflict of interest to declare?	No. The authors declare no conflict of interest.
Corresponding Author Secondary Information:	
Corresponding Author's Institution:	Peking University
Corresponding Author's Secondary Institution:	
First Author:	Shaojun Guo
First Author Secondary Information:	
Order of Authors:	Shaojun Guo
	Wei Wang, Dr
	Bo Jiang
	Chang Qian
	Fan Lv
	Jianrui Feng
	Jinhui Zhou
	Kai Wang
	Chao Yang
	Yong Yang
Order of Authors Secondary Information:	
Abstract:	Potassium-ion batteries (KIBs) are recently attracting intensive attention because of the abundant potassium resources and their low cost and high safety. However, the major challenge faced by KIBs lies on the lack of stable and high-capacity materials for the intercalation/deintercalation of large-size potassium ions. Herein, we synthesized a unique pistachio-shuck-like MoSe2/C core/shell nanostructure (PMC) as an advanced anode for boosting the performance of KIBs. This PMC features with a few layers of molybdenum selenide as the core with an expanded interlayer spacing of ca. 0.85 nm, facilitating the intercalation/deintercalation of K ions, and a thin amorphous carbon as the shell, which can confine the active molybdenum selenide nanosheets during cycling for maintaining the high structural stability. Most importantly, as a whole, the PMC has the advantages of reducing the surplus hollow interior space for improving its

	packing density and buffering the volume expansion during the K ion intercalation for further enhancing the stability. As a consequence, the PMC shows a very high capacity of 322 mAh g-1 at 0.2 A g-1 over 100 cycles, and can still remain 226 mAh g-1 at 1.0 A g-1 for a long period of 1000 cycles, which is among the best reported KIBs anodes.

WILEY-VCH

DOI: 10.1002/adma.((please add manuscript number))
Article type: Communication

Pistachio-Shuck-Like $MoSe_2$/C Core/Shell Nanostructures for High-Performance Potassium Ion Storage

*Wei Wang, Bo Jiang, Chang Qian, Fan Lv, Jianrui Feng, Jinhui Zhou, Kai Wang, Chao Yang, Yong Yang and Shaojun Guo**

Dr. W. Wang, C. Qian, F. Lv, J. Feng, J. Zhou, K. Wang, C. Yang, Dr. Y. Yang, Prof. S. Guo
Department of Materials Science and Engineering,
College of Engineering, Peking University,
Beijing 100871, China.
Email: guosj@pku.edu.cn

Dr. B. Jiang
Department of Materials Science and Engineering,
NTNU Norwegian University of Science and Technology,
Trondheim 7491, Norway.

Prof. S. Guo
BIC-ESAT, College of Engineering, Peking University, Beijing, 100871, China.
Beijing Key Laboratory for Magnetoeletric Materials and Devices (BKL-MEMD), Peking University, Beijing 100871, China.
Department of Energy and Resources Engineering, College of Engineering, Peking University, Beijing 100871, China.

Keywords: molybdenum selenide; potassium-ion battery; expanded interlayer spacing; high packing density

Abstract:

Potassium-ion batteries (KIBs) are recently attracting intensive attention because of the abundant potassium resources and their low cost and high safety. However, the major challenge faced by KIBs lies on the lack of stable and high-capacity materials for the intercalation/deintercalation of large-size potassium ions. Herein, we synthesized a unique pistachio-shuck-like $MoSe_2$/C core/shell nanostructure (PMC) as an advanced anode for

boosting the performance of KIBs. This PMC features with a few layers of molybdenum selenide as the core with an expanded interlayer spacing of ca. 0.85 nm, facilitating the intercalation/deintercalation of K ions, and a thin amorphous carbon as the shell, which can confine the active molybdenum selenide nanosheets during cycling for maintaining the high structural stability. Most importantly, as a whole, the PMC has the advantages of reducing the surplus hollow interior space for improving its packing density and buffering the volume expansion during the K ion intercalation for further enhancing the stability. As a consequence, the PMC shows a very high capacity of 322 mAh g^{-1} at 0.2 A g^{-1} over 100 cycles, and can still remain 226 mAh g^{-1} at 1.0 A g^{-1} for a long period of 1000 cycles, which is among the best reported KIBs anodes.

In virtue of their high energy and power densities, lithium-ion batteries (LIBs) have been widely used in portable electronics and electric vehicles.[1-3] However, the scarcity and uneven distribution of lithium source as well as its high cost largely limit the rapid growth of large-scale stationary application. Furthermore, the security issue caused by lithium dendrites is a big trouble in LIBs fields.[4,5] Therefore, developing low-cost, high-performance and high-security energy storage devices is of great significance as promising alternatives to LIBs, such as sodium-ion batteries (NIBs), magnesium-ion batteries (MIBs) and aluminum-based batteries (AGBs).[6-8] In recent three years, the new concept of potassium-ion batteries (KIBs) has become a hot spot in energy storage fields.[9] Compared with the natural abundance of lithium (20 ppm) in the earth's crust, the abundance of potassium (17000 ppm) seems inexhaustible.[10] Besides, the redox potential of K/K^+ (−2.93 V *vs* standard hydrogen electrode) is closer to that of Li/Li^+ (−3.04 V) than that of Na/Na^+ (−2.71 V), implying higher energy density in full cell. In this regards, KIBs show the promising prospect in large-scale stationary applications, and the researches on KIBs are still in early infancy. Generally, graphite is the most common anode for KIBs with a theoretical capacity of 279 mAh g^{-1}. Owing to their relatively large interlayer spacing (3.4 Å) and high electronic conductivity, a large amount of carbonaceous materials were investigated as anodes for KIBs.[11-13] Unfortunately, the stability and capacity retention are still not satisfied on account of the expansion and collapse of their crystal structure. Besides the carbonaceous materials, other noncarbonaceous materials were also explored, but their structures are usually seriously destroyed during cycling, greatly restricting the stability.[14-18]

Transition metal selenides, with the merits of transition metal chalcogenide for batteries including high capacity, intrinsically enhanced safety and high availability through the conversion

reaction[19,20] and also narrow-band-gap semiconductor characteristic, are superior anode for alkali-ion intercalation/deintercalation owing to their sandwich structure made up of stacked atom layers.[21] However, their large volume expansion after the intercalation of large-size K ion unavoidably impacts the cycling stability of KIBs. The flexible carbon matrix can buffer the volume variation, maintain the integrity of the electrode material, and meanwhile improve the electronic conductivity. Besides, the hollow nanostructures can sustain the large mechanical strain,[22-24] but their packing density is relatively low due to the surplus inner void space, leading to low volumetric energy and power densities of batteries.[25] In this regards, designing $MoSe_2$-carbon hollow structure analogue with high packing density is of much significance, however, achieving such target is still a great challenge.

Herein, we report the synthesis of a class of the pistachio-shuck-like $MoSe_2$/C core/shell nanostructure with an expanded $MoSe_2$ interlayer spacing of 0.85 nm as an advanced anode material for boosting the capacity, rate ability and cycling stability of KIBs. Compared with the common hollow structures with low packing density for battery (only point-to-point contact) (**Figure 1**a&b), the unique pistachio-shuck-like nanostructure can have better opportunity for enhancing the packing density (like plane-to-plane contact) (Figure 1c), which can not only facilitate the electronic transfer and K ion diffusion, but also maintain the structural stability during the charge and discharge process.[26,27] Besides, along the surface of carbon, the electrons can fluently pass from one side to another, and also the carbon can confine the formed molybdenum selenide nanosheets, further maintaining its structural stability, improving the rate behavior and cycling stability. As a result, after a long-time cycling of 1000 cycles, the PMC can still deliver a discharge capacity of 226 mAh g^{-1} at a very high current density of 1.0 A g^{-1}, among the best KIBs anodes reported. The first-principles calculations reveal that the energy barrier for the bulk molybdenum selenide is higher than the surface of expanded molybdenum selenide nanosheets, suggesting a faster diffusion of K ion in this unusual structure.

The synthetic process of PMC is schematically illustrated in Figure 1d. In a typical synthesis, 1.0 mmol sodium molybdate (Na_2MoO_4), 1.0 mmol dibenzyl diselenide (DBDS) and 10 mL oleylamine (OAm) were mixed together, then dried and degassed at 90 °C for 30 min under inert atmosphere. The mixture was heated to 250 °C with a heating rate of 8 °C min^{-1} for 30 min (holding time) and further heated to 550 °C for 2 h under inert atmosphere to get the PMC. We found that the holding time greatly impacts the morphology of molybdenum selenide nanostructures. The holding times of 5 min and 2 h led to the production of poor-crystallized nanospheres (NS) (Figure S1-3, Supporting Information) and the broken pistachio-shuck-like $MoSe_2$/C nanosheets (BPS) (Figure S4-6, Supporting Information).

The field-emission scanning electron microscopy (FESEM), high-angle annular dark-field imaging (HAADF)-scanning transmission electron microscopy (STEM) and transmission electron microscopy (TEM) images were used to characterize the PMC. It shows a pistachio-shuck-like morphology with a diameter of ca. 70-90 nm (**Figure 2**a, b, Figure S7&S8), and have the tap density of ca. 0.83 g cm^{-3}, higher than that (ca. 0.58 g cm^{-3}) of similar-particle-sized $MoSe_2$ nanoflowers (Figure S9, synthesized according to the previous report[28]). High-resolution transmission electron microscopy (HRTEM) image (Figure 2c) displays that the PMC is formed by stacking a few layers of molybdenum selenide nanosheets. An interesting thing for PMC is that an expanded interlayer spacing of ca. 0.85 nm is observed (Figure 2c and Figure S10 and S11, Supporting Information), larger than the previously reported value (ca. 0.65 nm) and that of similar-particle-sized $MoSe_2$ nanoflowers (ca. 0.64 nm),[29] probably owing to the intercalation of ammonium molecule derived from the OAm.[30,31] The bond length (Mo-Se) and bond angle (Se-Mo-Se) in bulk molybdenum selenide are 0.25 nm and 82.6°, respectively, and the thickness of one Se-Mo-Se layer is about 0.33 nm. Therefore, the gallery height between two neighboring layers in bulk molybdenum selenide is only 0.31 nm (Figure S12a, Supporting Information). Such an interlayer spacing is insufficient to accommodate K ions for fast intercalation/deintercalation reaction. When the interlayer spacing is enlarged to 0.85 nm, the gallery height is increased to 0.51 nm (Figure S12b, Supporting Information). The enlarged interlayer spacing can lower the energy barrier of K ion intercalation and diffusion and increase the number of exposed active sites for KIBs.[32] The surface of the "pistachio shuck" is coated with amorphous carbon, and the interiors are a few layers of curved nanosheets. The X-ray powder diffraction (XRD) pattern of PMC further validates the existence of molybdenum selenide and amorphous carbon (Figure S13, Supporting Information). It is noteworthy that the (002) diffraction peak shifts negatively compared with the bulk molybdenum selenide (14.1°), also demonstrating an enlarged interlayer spacing. The corresponding selected area electron diffraction (SAED) patterns (Figure S14, Supporting Information) also show the existence of crystalline molybdenum selenide and amorphous carbon. The HAADF-STEM image and energy dispersive X-ray spectra (EDS) elemental mapping (Figure 2d-f) results clearly reveal that the elements of Mo and Se are uniformly distributed throughout the PMC.

The X-ray photoelectron spectroscopy (XPS) was carried out to investigate the chemical composition and the surface electronic state of the as-obtained PMC (Figure 2g, h). The Mo 3d spectrum was well fitted by two peaks at 228.5 and 231.7 eV, respectively, being coincident with that of molybdenum selenide (Figure 2g).[33,34] Using the deconvolution method, the Se 3d spectrum was fitted by the assumption of two species at 54.3 and 55.2 eV, respectively (Figure 2h). The Raman spectrum of the as-obtained PMC shows the existence of carbon and molybdenum selenide (Figure

S15, Supporting Information).[34] It can be clearly seen that the D-band (assigned to A_{1g} vibration mode of sp^2 carbon rings caused by defects) is more intensive than the G-band (assigned to E_{2g} vibration mode of sp^2 carbon atoms) with a I_D/I_G value of 1.19, indicating its amorphous nature. Based on the above analysis, the schematic diagram of the cross-sectional view for PMC is drawn in Figure 2i.

Electrochemical measurements were carried out using the CR2032-type coin cells. The electrochemical process of K-ion intercalation and deintercalation of PMC was investigated by cyclic voltammetry (CV) (Figure S16, Supporting Information). In the first cycle, three reduction peaks at 1.56, 1.22 and 0.55 V can be clearly seen, which are associated with the intercalation of K ions into the $MoSe_2$ crystal and the formation of K_xMoSe_2, the conversion reaction from K_xMoSe_2 to Mo and the formation of the solid electrolyte interphase (SEI) layer on the PMC surface, respectively.[35,36] **Figure 3**a shows the galvanostatic charge/discharge curves of the PMC. The first charge/discharge curves are separated out (Figure S17, Supporting Information) to get a clear view. The charge/discharge capacities for the first cycle are 402 and 635 mAh g^{-1}, respectively, with a Coulombic efficiency of 63.4%. The particularly high capacity and the remarkable capacity loss between the initial and second cycles is mainly attributed to some irreversible processes like the formation of the SEI layer on the PMC surface,[37] agreeing well with the results of the CV curves. As a comparison, the curve shape of BPS is similar to that of PMC except for the fast capacity decay, caused by the fragmentized nanosheets and aggregation (Figure S18a, Supporting Information) whereas the NS shows a different profile owing to its poor-crystallized state (Figure S18b, Supporting Information).

The charge/discharge capacity and Coulombic efficiency of the PMC at 0.2 A g^{-1} over 100 cycles are displayed in Figure 3b. The capacities for the initial three cycles are particularly higher than those for other cycles, and the capacity fading is obvious, attributed to the side reaction. In the subsequent cycles, high capacity retention and Coulombic efficiency were obtained, indicating a high reversibility during cycling. After 100 cycles, the capacity can still remain 322 mAh g^{-1}. The PMC can also achieve the highly reversible capacity retention of approximately 83.9%, demonstrating its good cycling stability. In the meantime, the low-cutoff potential at 0.5 V was also measured. Obvious charge/discharge plateaus could be seen, however, its capacity is lower than that with low-cutoff potential at 0.01 V (Figure S19, Supporting Information). Although deep discharge may cause more damage to the electrode, however, owing to the unique structure, the cycling stability with low-cutoff potential at 0.01 V is comparable to that with low-cutoff potential at 0.5 V (Figure S20, Supporting Information).

The comparison of the cycling stability of NS, PMC and BPS for KIBs at 0.2 A g^{-1} was shown

in Figure 3c. Apparently, the PMC displays the best capacity and cycling stability among NS, PMC and BPS. Likewise, the PMC exhibits much better rate performance than the NS and BPS under different current densities from 0.2 to 2.0 A g^{-1} (Figure 3d). Reversible capacities of 382, 342, 304, 277, 254 and 224 mAh g^{-1} are obtained after increasing the charge/discharge current densities from 0.2 A g^{-1} to 0.4, 0.6, 0.8, 1.0 and 2.0 A g^{-1}. It's worth noting that even over 60 cycles under different current densities, the capacity can still be restored to 345 mAh g^{-1} when the current density returns to 0.2 A g^{-1}, demonstrating superior rate performance and cycling reversibility. Meanwhile, the PMC also exhibits superior capacity retention under different current densities (Figure S21, Supporting Information).

Figure 3e shows the long-term cycling stability of PMC at a very high current density of 1.0 A g^{-1} over 1000 cycles. After such a long-time cycling, a high discharge capacity of 226 mAh g^{-1} can be still maintained, which is one of the best reported KIBs anodes (Table S1). It is noteworthy that after the initial several cycles, the Coulombic efficiency increases to approximately 100%, indicating a superior reversibility during charge/discharge process. The reversible capacity retention of 83.5% is achieved, with a tiny capacity fading of ca. 0.017% *per* cycle. A clear outline of the morphology by FESEM and TEM observation after 1000 cycles reveals the structural stability during cycling (Figure S22, Supporting Information).

The electrochemical impedance spectroscopy (EIS) of the PMC was performed for the original, 5^{th} and 100^{th} cycles within a frequency range from 100 kHz to 0.01 Hz (Figure S23, Supporting Information). Generally for batteries, each impedance spectrum falls into two parts: i) a depressed semicircle at high frequency is attributed to the charge-transfer impedance and ii) a slope line of 45° at low frequency is ascribed to the semi-infinite diffusion of alkali ions into the electrode/electrolyte interface. The fresh battery shows a high impedance due to its inactivity before cycling. After being cycled for 5 and 100 cycles, the impedances of both become lower than that of the fresh one, and the 5^{th} and 100^{th} curves almost overlap with each other, indicating its good reversibility. Unlike ordinary batteries with a slope line of 45° at low frequency, the PMC appears a much steeper curve, demonstrating its capacitive character.[38] The EIS data were also fitted by the equivalent circuit. R_1 represents the internal resistance of the coin-cell battery and C1 represents the capacitance. W_1 is associated with the Warburg impedance, corresponding to the potassium-diffusion process. R_{ct} and CPE are related to the charge-transfer resistance and the constant phase-angle element that involves double layer capacitance. The impedance parameters of PMC after different cycles are listed in Table S2 (Supporting Information). From the 5^{th} cycle to 100^{th} cycle, only litter change of the charge-transfer resistance can be observed, indicating good structural stability during cycling.

To further prove the capacitive behavior, the CVs were carried out at stepped scan rates from

0.1 to 1.2 mV s^{-1} in a voltage range from 0.01 to 2.5 V (**Figure 4**a). According to the previous reports,[39] the peak current (i) and the scan rate (υ) abide by the relationship of $i = av^b$. In the meantime, the b value can be obtained by the slope of the log (i) *vs.* log(υ) plot (Figure S24a, Supporting Information). When the b value is close to 0.5, the electrochemical behavior is dominated by the ionic diffusion process, while the b value close to 1.0 indicates a total capacitive process.[40] To be specific, the capacitive contribution ratio under different scan rates can be quantified through the Equation of $i = k_1v + k_2v^{1/2}$, where k_1v and $k_2v^{1/2}$ represent the contribution of capacitance and ionic diffusion, respectively.[39] When charging at a low scan rate of 0.1 mV s^{-1}, the b value is below 0.5, indicating the charge storage behavior is dominated by the ionic diffusion process (Figure S24b, Supporting Information). As the scanning rate increases, the capacitive charge contribution becomes higher and finally reaches the maximum value of 76% at a high scan rate of 1.2 mV s^{-1} (Figure 4b). Under this scan rate, the capacity contribution is dominated by capacitive behavior.

The reasons for the excellent K-ion storage are as follows. i) Usually the hollow nanostructures have the advantages of the accommodation of the volume expansion during cycling, but have to face the shortcoming of low volumetric energy and power densities. The pistachio-shuck-like nanostructure inherits the above-mentioned merits and overcomes the shortcoming of hollow nanostructure. This unusual structure can be packed more closely and reduce the surplus hollow interior space (Figure 1b). Compared with the hollow nanospheres, this pistachio-shuck-like nanostructure has more interfacial contact between the adjacent particles and also more contact area with the electrolyte, which can improve the electronic transmission and K ion diffusion as well as maintain the structural stability. ii) The large interlayer spacing can facilitate the transmission of K ion and accommodate the volume expansion during cycling. At a high charge/discharge current density of 0.5 A g^{-1}, $MoSe_2$ nanoflowers with smaller interlayer spacing (0.64 nm) and similar particle size show the lower capacity and poorer stability (Figure S25, Supporting Information), further proving the advantage of large interlayer spacing and the unique structure of PMC in boosting KIBs. iii) Usually the transition metal sulfide is semiconductor, while the bandgap of molybdenum selenide is much smaller, endowing it with relatively high electronic conduction. Besides, the electrons can easily transfer along the carbon coated on the PMC surface, improving the rate capability (Figure S26, Supporting Information). iv) The surface carbon could confine the formed molybdenum selenide nanosheets and maintain its structural stability during the charge/discharge process. v) The non-ignorable capacitive contribution is another significant factor in achieving high capacity.

In order to better understand the intercalation process, the possible migration pathways for potassium diffusion in the bulk and on the surface of molybdenum selenide were investigated by first

principles. The surface structure can be approximately treated as the expanded interlayer spacing in molybdenum selenide structure, which makes it easy for comparisons. The potassium has two intercalation sites: the hollow octahedral (O_h) and the top tetrahedral (T_d) site[41,42] in molybdenum selenide structure (Figure 4c, d). The relative energies of the diffusion along the two kinds of pathways are presented in Figure 4e. The potassium intercalation is energetic favorability to the (O_h) sites in bulk molybdenum selenide, while the surface of molybdenum selenide represents an opposite trend. The energy barrier from climbing-image nudged elastic band method (cNEB) calculations for the bulk molybdenum selenide is higher than the surface of molybdenum selenide, similar to the results of the sodium ion diffusion trajectories in molybdenum selenide.[43] This result suggests a faster diffusion of K ion on the layer than in the bulk molybdenum selenide. Further investigation of bond structure also suggests the transformation from semiconductor to metal after potassium intercalation, indicating a higher electronic conductivity (Figure S27, Supporting Information).

In summary, we synthesized a new class of pistachio-shuck-like $MoSe_2$/C core/shell nanostructure with an expanded $MoSe_2$ interlayer spacing as an advanced anode material for enhancing the performance of KIBs. This unique structure is expected to be packed closely for not only improving the K ion diffusion and electronic transfer, but also enhancing the volumetric energy density. These important new features make PMC deliver a high capacity of 322 mAh g^{-1} over 100 cycles with the reversible capacity retention of approximately 83.9%. When cycled at a very high current density of 1.0 A g^{-1} and for a long period of 1000 cycles, the capacity can still retain 226 mAh g^{-1}, with a capacity fading of only 0.017% *per* cycle, demonstrating superior rate performance and cycling stability. The first-principles calculations reveal a low energy barrier during K-ion intercalation, corroborating the high-rate performance in this unusual structure.

Supporting Information

Supporting Information is available from the Wiley Online Library or from the author.

Acknowledgements.

This work was financially supported by the National Key Research and Development Program of China (No. 2016YFB0100201), the National Natural Science Foundation of China (51671003), the start-up supports from Peking University and Young Thousand Talented Program and China Postdoctoral Science Foundation (2016M600013).

Conflict of Interest

The authors declare no conflict of interest.

Received: ((will be filled in by the editorial staff))
Revised: ((will be filled in by the editorial staff))
Published online: ((will be filled in by the editorial staff))

References

[1] B. Dunn, H. Kamath, J.-M. Tarascon, *Science* **2011**, *334*, 928.

[2] A. S. Arico, P. Bruce, B. Scrosati, J.-M. Tarascon, W. Van Schalkwijk, *Nat. Mater.* **2005**, *4*, 366.

[3] Y. Zou, S. Chen, X. Yang, N. Ma, Y. Xia, D. Yang, S. Guo, *Adv. Energy Mater.* **2016**, *6*, 1601549

[4] N. Yabuuchi, K. Kubota, M. Dahbi, S. Komaba, *Chem. Rev.* **2014**, *114*, 11636.

[5] N. Yabuuchi, M. Kajiyama, J. Iwatate, H. Nishikawa, S. Hitomi, R. Okuyama, R. Usui, Y. Yamada, S. Komaba, *Nat. Mater.* **2012**, *11*, 512.

[6] T. Sun, Z. j. Li, H. g. Wang, D. Bao, F. l. Meng, X. b. Zhang, *Angew. Chem. Int. Ed.* **2016**, *128*, 10820.

[7] K. W. Nam, S. Kim, S. Lee, M. Salama, I. Shterenberg, Y. Gofer, J.-S. Kim, E. Yang, C. S. Park, J.-S. Kim, *Nano Lett.* **2015**, *15*, 4071.

[8] W. Wang, B. Jiang, W. Xiong, H. Sun, Z. Lin, L. Hu, J. Tu, J. Hou, H. Zhu, S. Jiao, *Sci. Rep.* **2013**, *3*, 3383.

[9] A. Eftekhari, Z. Jian, X. Ji, *ACS Appl. Mater. Inter.* **2016**, *9*, 4404.

[10]D. Larcher, J.-M. Tarascon, *Nat. Chem.* **2015**, *7*, 19.

[11] Z. Jian, W. Luo, X. Ji, *J. Am. Chem. Soc.* **2015**, *137*, 11566.

[12] Z. Jian, Z. Xing, C. Bommier, Z. Li, X. Ji, *Adv. Energy Mater.* **2016**, *6*, 1501874.

[13] W. Luo, J. Wan, B. Ozdemir, W. Bao, Y. Chen, J. Dai, H. Lin, Y. Xu, F. Gu, V. Barone, *Nano Lett.* **2015**, *15*, 7671.

[14] W. Zhang, J. Mao, S. Li, Z. Chen, Z. Guo, *J. Am. Chem. Soc.* **2017**, *139*, 3316.

[15] P. Lian, Y. Dong, Z.-S. Wu, S. Zheng, X. Wang, S. Wang, C. Sun, J. Qin, X. Shi, X. Bao, *Nano Energy* **2017**, *40*, 1.

[16] B. Kishore, G. Venkatesh, N. Munichandraiah, *J. Electrochem. Soc.* **2016**, *163*, A2551.

[17] J. Han, M. Xu, Y. Niu, G.-N. Li, M. Wang, Y. Zhang, M. Jia, C. M Li, *Chem. Commun.* **2016**, *52*, 11274.

[18] Y. An, H. Fei, Z. Zhang, L. Ci, S. Xiong, J. Feng, *Chem. Commun.* **2017**, *53*, 8360.

[19] X. Y. Yu, H. Hu, Y. Wang, H. Chen, X. W. D. Lou, *Angew. Chem. Int. Ed.* **2015**, *54*, 7395.

[20] R. Wu, D. P. Wang, X. Rui, B. Liu, K. Zhou, A. W. Law, Q. Yan, J. Wei, Z. Chen, *Adv. Mater.*

2015, *27*, 3038.

[21] R. Tenne, L. Margulis, M. Genut, G. Hodes, *Nature* **1992**, *360*, 444.

[22] J. Ye, H. Zhang, R.Yang, X. Li, L. Qi, *Small* **2010**, *6*, 296.

[23] L. Zhang, H. B. Wu, B. Liu, X. W. D. Lou, *Energy Environ. Sci.* **2014**, *7*, 1013.

[24] S. Ding, J. S. Chen, G. Qi, X. Duan, Z. Wang, E. P. Giannelis, L. A. Archer, X. W. Lou, *J. Am. Chem. Soc.* **2011**, *133*, 21.

[25] J. Liang, X.-Y. Yu, H. Zhou, H. B. Wu, S. Ding, X. W. D. Lou, *Angew. Chem. Int. Ed.* **2014**, *53*, 12803.

[26] L. Zhang, H. B. Wu, B. Liu, X. W. D. Lou, *Energy Environ. Sci.* **2014**, *7*, 1013.

[27] Y. Fang, Y. Lv, F. Gong, Z. Wu, X. Li, H. Zhu, L. Zhou, C. Yao, F. Zhang, G. Zheng, *J. Am. Chem. Soc.* **2015**, *137*, 2808.

[28] Z. Liu, N. Li, H. Zhao, Y. Du, *J. Mater. Chem. A* **2015**, *3*, 19706.

[29] P. Liu, J. Zhu, J. Zhang, P. Xi, K. Tao, D. Gao, D. Xue, *ACS Energy Lett.* **2017**, *2*, 745.

[30] J. Feng, X. Sun, C. Wu, L. Peng, C. Lin, S. Hu, J. Yang, Y. Xie, *J. Am. Chem. Soc.* **2011**, *133*, 17832.

[31] Q. Liu, X. Li, Q. He, A. Khalil, D. Liu, T. Xiang, X. Wu, L. Song, *Small* **2015**, *11*, 5556.

[32] J. Zhang, M. Wu, T. Liu, W. Kang, J. Xu, *J. Mater. Chem. A* **2017**, *5*, 24859.

[33] X. Wang, Y. Gong, G. Shi, W. L. Chow, K. Keyshar, G. Ye, R. Vajtai, J. Lou, Z. Liu, E. Ringe, *ACS Nano* **2014**, *8*, 5125.

[34] D. Sun, S. Feng, M. Terrones, R. E. Schaak, *Chem. Mater.* **2015**, *27*, 3167.

[35] L. Yang, S. Wang, J. Mao, J. Deng, Q. Gao, Y. Tang, O. G. Schmidt, *Adv. Mater.* **2013**, *25*, 1180.

[36] K. Chang, D. Geng, X. Li, J. Yang, Y. Tang, M. Cai, R. Li, X. Sun, *Adv. Energy Mater.* **2013**, *3*, 839.

[37] K. Chang, W. Chen, *ACS Nano* **2011**, *5*, 4720.

[38] L. Cao, F. Xu, Y. Y. Liang, H. L. Li, *Adv. Mater.* **2004**, *16*, 1853.

[39] D. Su, A. McDonagh, S. Z. Qiao, G. Wang, *Adv. Mater.* **2017**, *29*, 1604007.

[40] J. Wang, H. Tang, L. Zhang, H. Ren, R. Yu, Q. Jin, J. Qi, D. Mao, M. Yang, Y. Wang, *Nat. Energy* 2016, *1*, 16050.

[41] Q. Li, Z. Yao, J. Wu, S. Mitra, S. Hao, T. S. Sahu, Y. Li, C. Wolverton, V. P. Dravid, *Nano Energy* **2017**, *38*, 342.

[42] H. Wang, X. Wang, L. Wang, J. Wang, D. Jiang, G. Li, Y. Zhang, H. Zhong, Y. Jiang, *J. Phys. Chem. C* **2015**, *119*, 10197.

[43] H. Wang, X. Lan, D. Jiang, Y. Zhang, H. Zhong, Z. Zhang, Y. Jiang, *J. Power Sources* **2015**, *283*, 187.

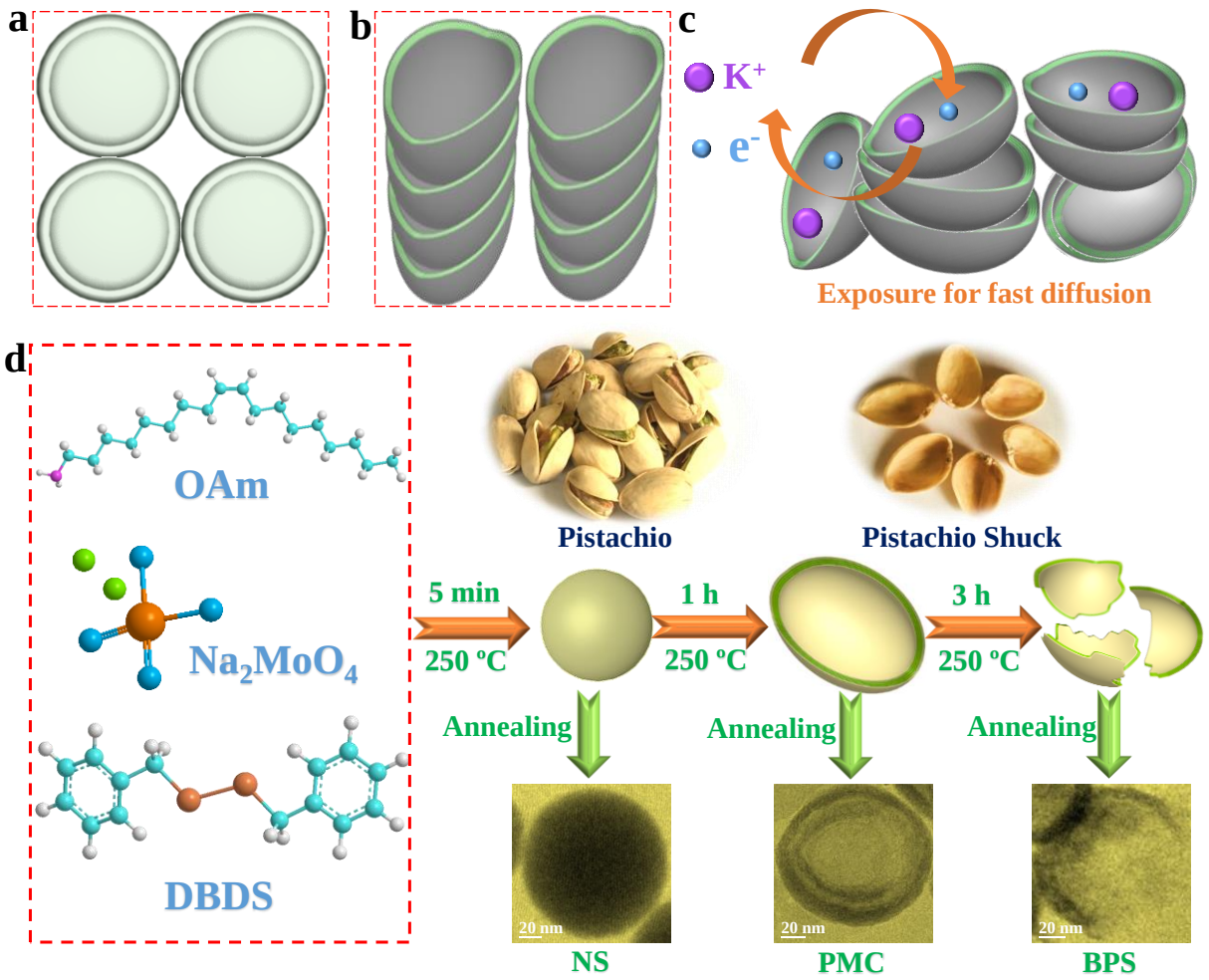

Figure 1. The comparison of packing of (a) hollow nanospheres and (b) PMC for KIBs. (c) Schematic diagram of fast ion and electron diffusion in PMC. (d) Synthetic conditions and morphologies of different molybdenum selenide-based nanostructures.

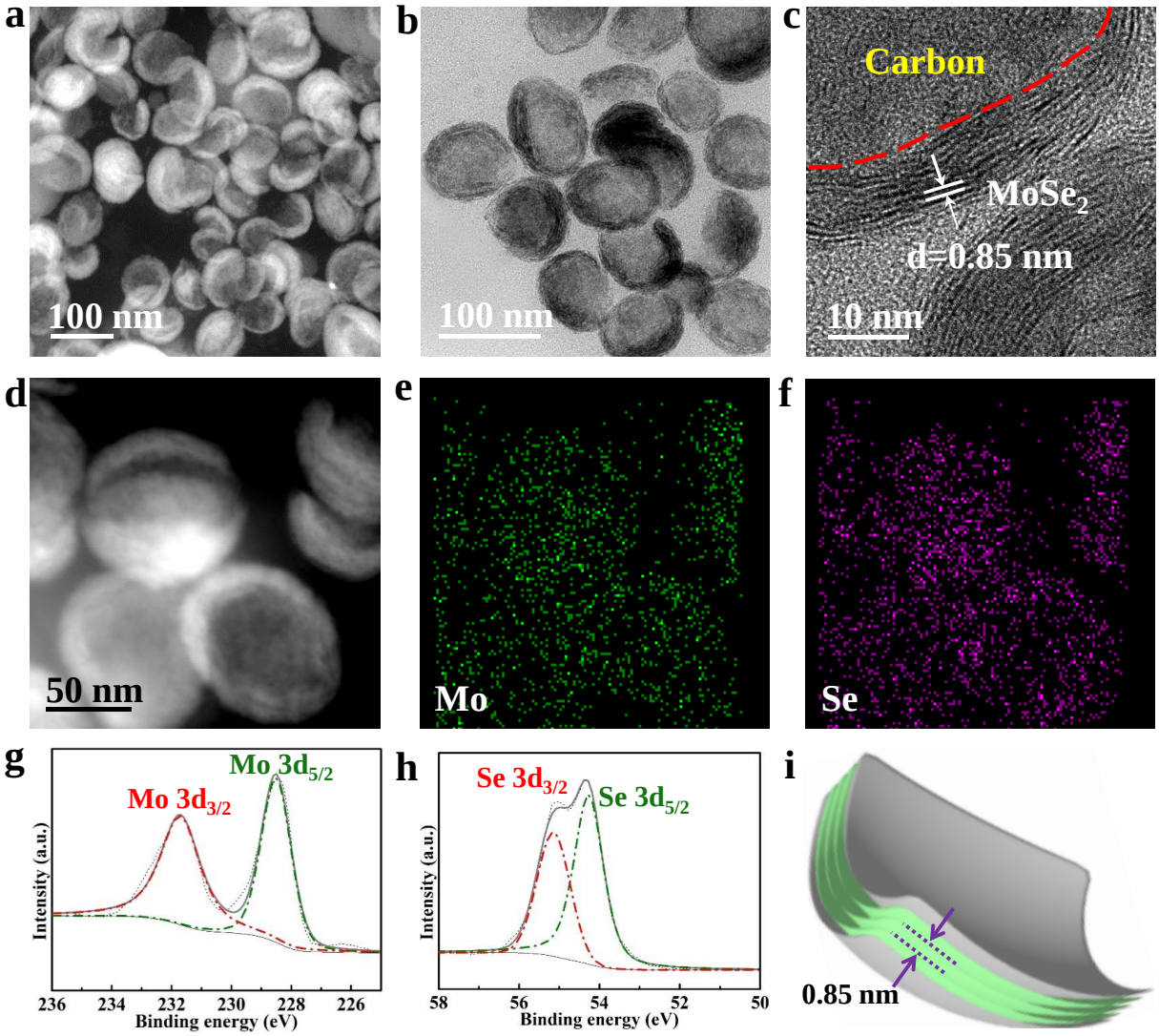

Figure 2. (a) HAADF-STEM, (b) TEM and (c) HRTEM images of the PMC. (d) HAADF-STEM image and the corresponding EDS mappings of (e) Mo and (f) Se. XPS spectra of (g) Mo 3d and (h) Se 3d in PMC. (i) Schematic diagram of the cross-sectional view for PMC.

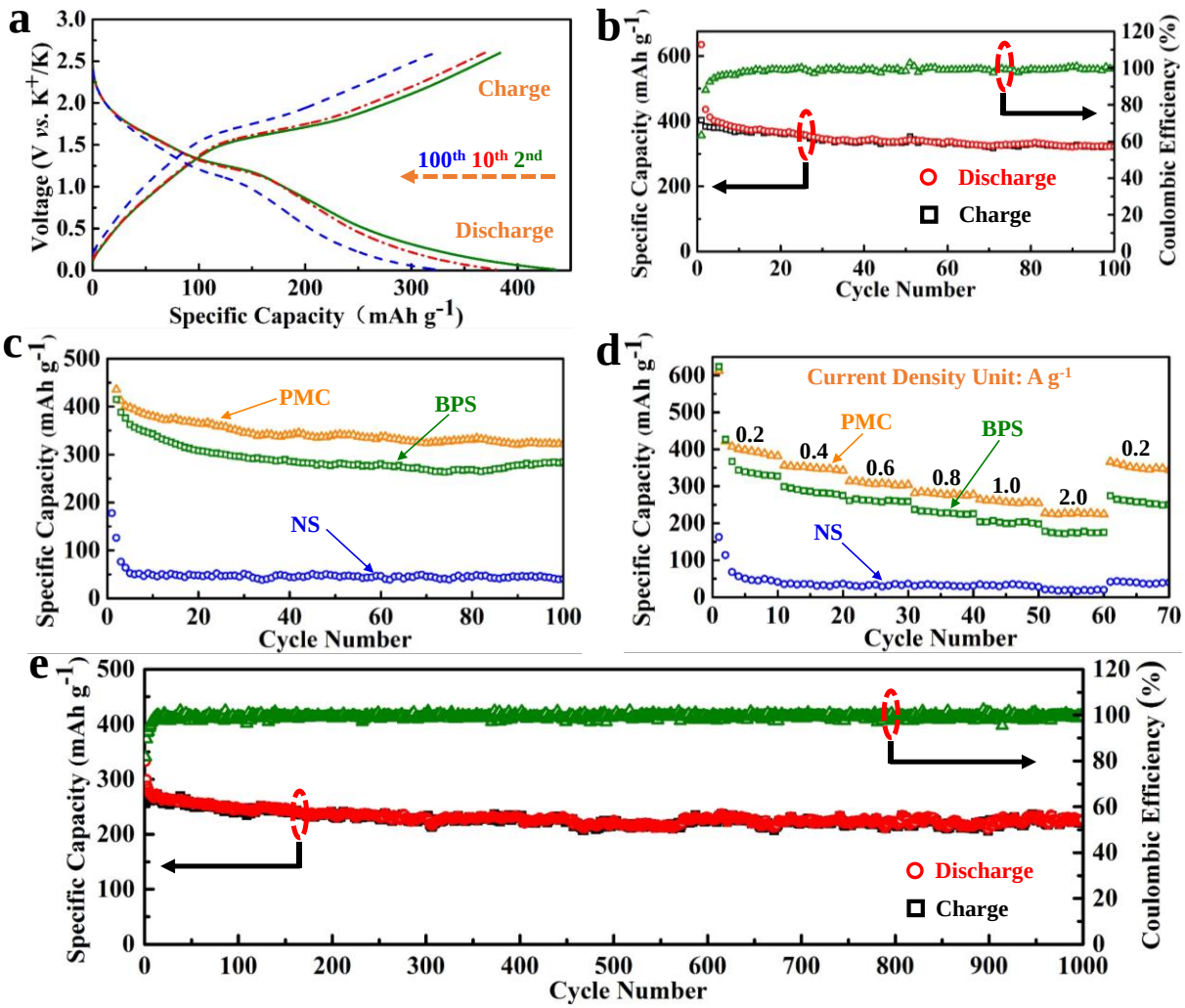

Figure 3. (a) The 2nd, 10th and 100th charge/discharge curves of PMC at 0.2 A g^{-1} for KIBs. (b) Charge/discharge capacity and Coulombic efficiency of PMC at 0.2 A g^{-1}. Comparison of (c) cycling stability and (d) rate performance under different current densities of the as-prepared NS, PMC and BPS. (e) Long-term cycling stability and Coulombic efficiency at a high current density of 1.0 A g^{-1} over 1000 cycles.

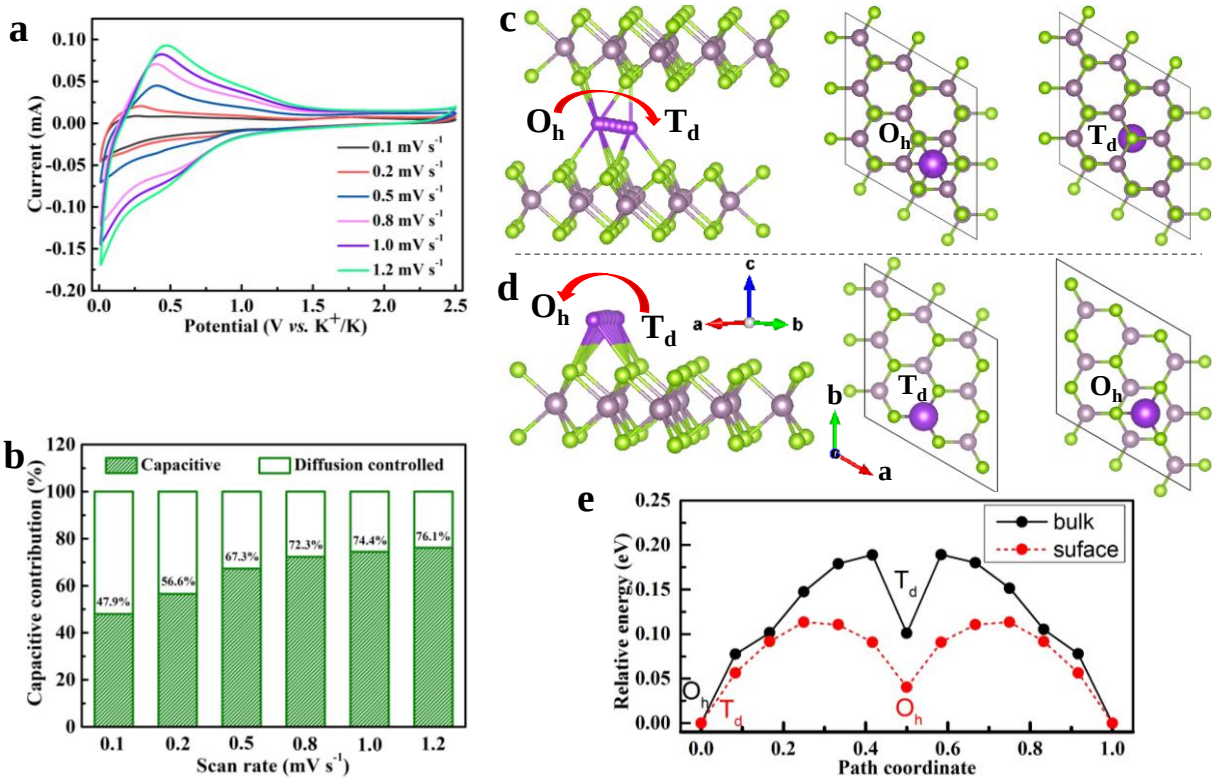

Figure 4. (a) CV profiles at different scan rates and (b) the corresponding percentage of pseudocapacitive contribution. The K migration paths in the bulk (c) and on the surface (d) of molybdenum selenide. (e) Relative energies along the two kinds of pathways.

A unique pistachio-shuck-like molybdenum selenide/carbon core/shell nanostructure (PMC) is synthesized as an advanced KIBs anode for boosting the performance in terms of capacity, rate ability and cycling stability. The superior performance is owing to the expanded interlayer spacing, high packing density and molybdenum selenide/carbon core/shell structure.

Wei Wang, Bo Jiang, Chang Qian, Fan Lv, Jianrui Feng, Jinhui Zhou, Kai Wang, Chao Yang, Yong Yang and Shaojun Guo*

Pistachio-Shuck-Like $MoSe_2$/C Core/Shell Nanostructures for High-Performance Potassium Ion Storage

TOC figure

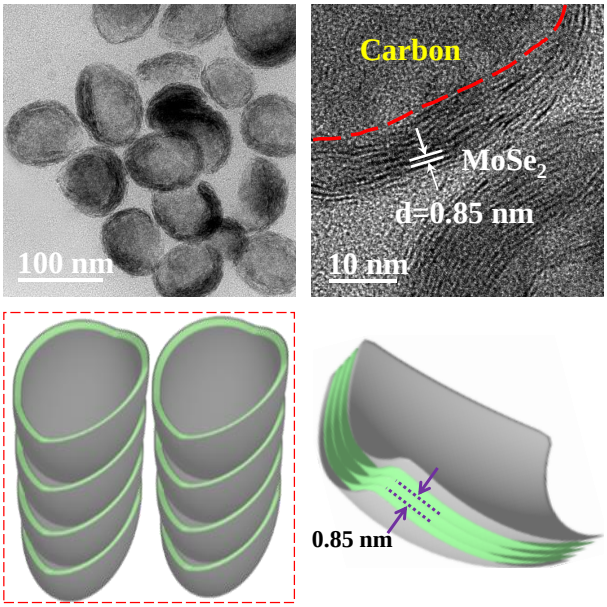

Figures

Table of Contents